Supplementary information

Enhanced photocatalytic H_2 evolution and H_2O_2 generation via $ZnIn_2S_4$/g-C_3N_4 heterojunction

Li Zhou[b,†], Yanming Zhou[b,†], Yujie Jia[b], Qiqi Gu[b], Qiaoyi Xiao[b], Xiao Wang[c], Suping Zhang[a,*], Hongmei Wang[b,*]

[a] *College of Fashion and Design, Jiaxing Nanhu University, Jiaxing 314001, China*
[b] *College of Biological, Chemical Sciences and Engineering, Jiaxing University, Jiaxing 314001, China*
[c] *School of Physics, East China University of Science and Technology, Shanghai 200237, China*

1. Experimental section

1.1 Characterization

The crystalline structure of the sample was determined by X-ray diffraction (XRD, Shimadzu XRD-7000) with Cu K_α radiation (λ = 1.5406 Å) over the 2θ range of 10°-80° at a scanning rate of 5°/min. Morphological and microstructural analyses were performed using transmission electron microscopy (TEM, Thermo Fisher Scientific Talos F200X) operated at 200 kV. For TEM observation, the sample was first dispersed in anhydrous ethanol via ultrasonication, deposited onto a carbon-coated copper grid, and then dried at ambient temperature. The surface elemental chemical states of the sample were analyzed using an X-ray photoelectron spectrometer (Thermo Fisher Scientific ESCALAB 250Xi, Al K_α radiation), with binding energies calibrated using the C 1s peak (284.8 eV). The optical absorption properties of the sample were tested using a UV-Vis spectrophotometer (Agilent Cary 5000, $BaSO_4$ as reference) in the wavelength range of 200-800 nm. The absorption spectra were derived from diffuse reflectance data by applying the Kubelka-Munk transformation. were tested by FLS980 (Edinburgh, Britain). The superoxide radical was analyzed using electron spin resonance (ESR, Bruker EMXplus) spectroscopy. Photoluminescence (PL) spectra and the transient fluorescence decay curves of the sample were measured at room temperature using a time-resolved fluorescence spectrometer (Edinburgh Instruments FLS980, excitation wavelength 375 nm), and the fluorescence lifetime was obtained by fitting the data with an exponential decay function.

1.2 Photoelectrochemical tests

Photoelectrochemical (PEC) measurements were carried out on a CHI660E electrochemical workstation (Shanghai Chenhua, China). The photocurrent response, electrochemical impedance spectroscopy (EIS), and Mott-Schottky (M-S) plots were recorded using a conventional three-electrode configuration in 0.2 M Na_2SO_4 electrolyte. A Pt plate and an Ag/AgCl electrode served as the counter and reference electrodes, respectively. The working electrode was fabricated by depositing the sample onto fluorine-doped tin oxide (FTO) glass. For electrode preparation, 5 mg of the catalyst was uniformly dispersed in a solution containing 950 μL isopropanol and 50 μL Nafion under ultrasonication. Then, 30 μL of the resulting suspension was drop-cast onto the FTO substrate and dried naturally in air to obtain the working electrode.

1.3 Active species trapping experiment

To investigate the main active species involved in the photocatalytic H_2O_2 production process, silver nitrate ($AgNO_3$), 1,4-benzoquinone (BQ), and ethylenediaminetetraacetic acid (EDTA) were used to trap electrons (e^-), superoxide radicals ($\cdot O_2^-$), and holes (h^+), respectively, at the same concentration (0.500 mM). The specific procedure involved adding $AgNO_3$, BQ, and EDTA to the reaction solution during the photocatalytic H_2O_2 production process, while the remaining steps followed the standard procedure for hydrogen peroxide preparation. The active species trapping experiments were conducted to identify the key active species responsible for the photocatalytic H_2O_2 production, thereby supporting the proposed photocatalytic reaction mechanism.

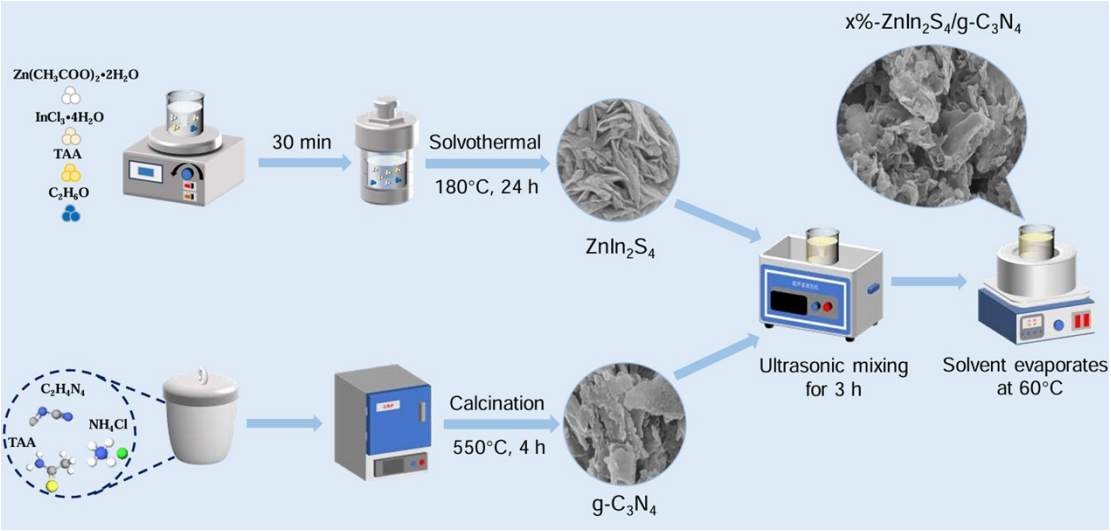

Figure S1 Schematic illustration of the synthesis process of the x%-$ZnIn_2S_4$/g-C_3N_4 nanocomposites.

2. Results and Discussion

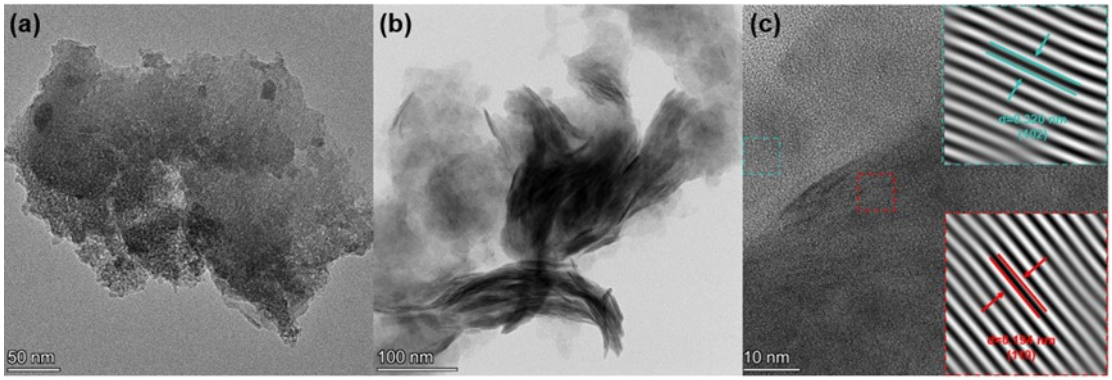

Figure S2 (a) TEM image of pure g-C_3N_4; (b) TEM image of pure $ZnIn_2S_4$; (c) HRTEM image of pure $ZnIn_2S_4$.

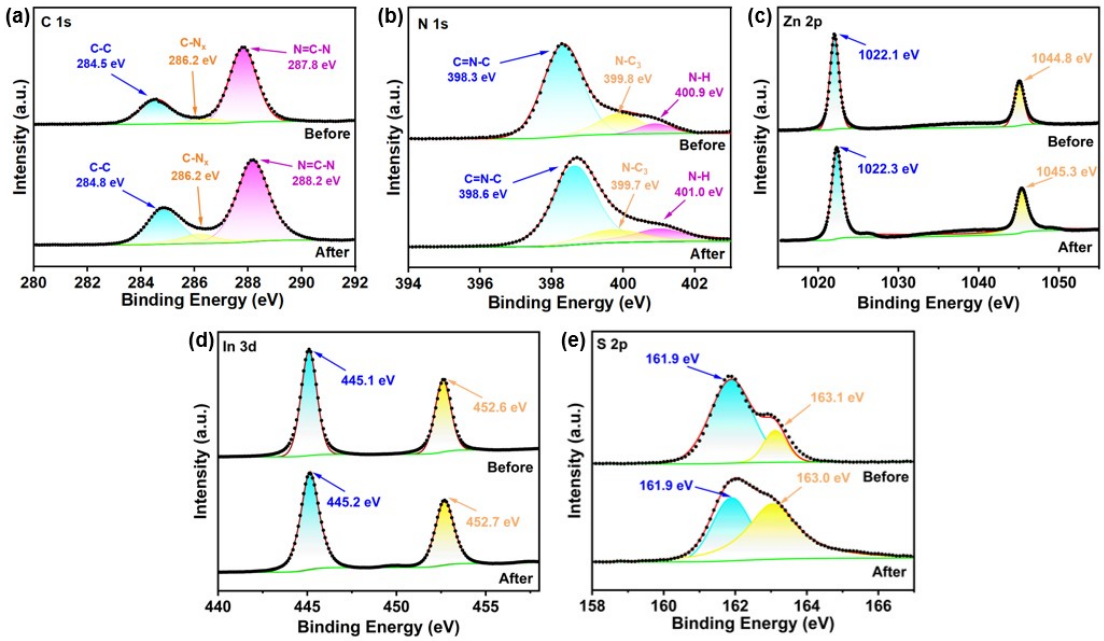

Figure S3 XPS results of (a) C 1s; (b) N 1s; (c) Zn 2p; (d) In 3d; (e) S 2p of 7%-$ZnIn_2S_4$/g-C_3N_4 nanocomposite before and after cycle photocatalysis.

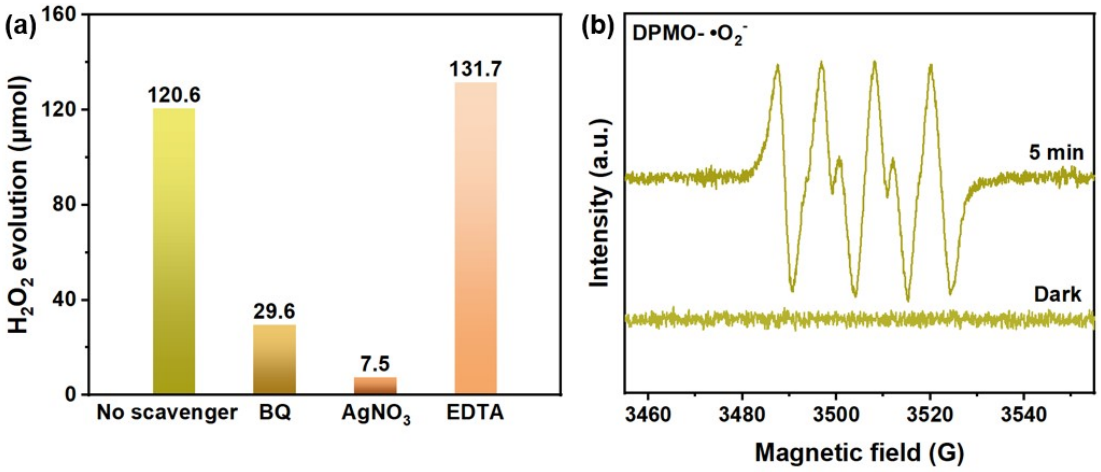

Figure S4 (a) Active species capture experiment of photocatalytic generation of H_2O_2; (b) ESR spectra of 7%-$ZnIn_2S_4$/g-C_3N_4.

Table S1 Photocatalytic performance comparison of 7%-$ZnIn_2S_4$/g-C_3N_4 with reported materials for H_2 production.

Photocatalyst	Light	Sacrificial reagent	Catalyst mass (mg)	Hydrogen production rate ($\mu mol \cdot g^{-1} \cdot h^{-1}$)	Reference
7%-$ZnIn_2S_4$/g-C_3N_4	300 W Xe lamp	TEOA, 15 vol.%	30	1869.1	This work
40% CPMV/CN	300 W Xe lamp	DL-lactic acid, 10 vol.%	20	1515.63	[R1]
$CuS_{0.5}Se_{0.5}$/g-C_3N_4	300 W Xe lamp	TEOA, 20 vol.%	10	1327.3	[R2]
CN/CT-Mn	300 W Xe lamp	MeOH, 10 vol.%	20	720	[R3]
CNV-1	125 W Xe lamp	MeOH, 10 vol.%	20	981	[R4]
ZnO/Mo_2C-3/PAH	300 W Xe lamp	/	/	755.5	[R5]
B-Red P/BN	300 W Xe lamp	/	20	212.5	[R6]
TC@TO/NCL-20	125 W Xe lamp	MeOH, 10 vol.%	20	593	[R7]
EZUNH-2	300 W Xe lamp	MeOH, 10 vol.%	20	331.26	[R8]
NCP@ZIS@Co	300 W Xe lamp	/	10	1541.2	[R9]
α-MnO_2@B/O-g-C_3N_4/d-Ti_3C_2	150 W Xe lamp	MeOH, 10 vol.%	20	897.2	[R10]

12-NOCN	300 W Xe lamp	TEOA, 10 vol.%	40	112.2	[R11]
g-C_3N_4/AIS	300 W Xe lamp	/	30	237	[R12]
WS_2/S-g-C_3N_4	300 W Xe lamp	Rh B solution, 10 vol.%	10	1380	[R13]
Bina-CN	300 W Xe lamp	TEOA, 10 vol.%	200	970	[R14]
In_2S_3	300 W Xe lamp	/	30	42.17	[R15]

Table S2 Photocatalytic performance comparison of 7%-$ZnIn_2S_4$/g-C_3N_4 with reported materials for H_2O_2 production.

Photocatalyst	Light	Atmosphere	Condition	Hydrogen peroxide production rate ($\mu mol \cdot g^{-1} \cdot h^{-1}$)	Reference
7%-$ZnIn_2S_4$/g-C_3N_4	300 W Xe lamp	O_2	10 vol% IPA	803.8	This work
40% CPMV/CN	300 W Xe lamp	O_2	10 vol% EtOH	1400	[R1]
CN/CT-Mn	300 W Xe lamp	O_2	10 vol% MeOH	104	[R3]
CNV-1	250W Hg Lamp/	O_2	5 vol% IPA	1867.5	[R4]
ZnO/Mo_2C-3/PAH	300 W Xe lamp	/	/	626.3	[R5]
B-Red P/BN	300 W Xe lamp	/	/	172	[R6]
TC@TO/NCL-20	125 W Xe lamp	O_2	5 vol% IPA	1183	[R7]
EZUNH-2	300 W Xe lamp	O_2	5 vol% IPA	35.2	[R8]
NCP@ZIS@Co	300 W Xe lamp	/	/	1381.1	[R9]
α-MnO_2@B/O-g-C_3N_4/d-Ti_3C_2	250 W Xe lamp	O_2	10 vol% EtOH	2846.4	[R10]
12-NOCN	300 W Xe lamp	Air	10 vol% IPA	91.2	[R11]
2% Ru-ZIS	300 W Xe lamp	/	/	464.4	[R16]
1% TC/g-CN/BOC	300 W Xe lamp	O_2	5 vol% IPA	664.05	[R17]
e-BCN	250 W Xe	O_2	5 vol%	398.3	[R18]

	lamp		EtOH		
WO_3/NiS	300 W Xe lamp	Air	/	619	[R19]
CdS/CFR-15	300 W Xe lamp	O_2	/	275	[R20]

References

[R1] Y. Zhai, T. Zhao, X. Zhou, et al. Construction of $Cs_5PMo_{10}V_2O_{40}$/g-C_3N_4 S-scheme heterojunction with boosted photocatalytic properties for H_2O_2 and H_2 production. Appl. Surf. Sci., 2026, 728: 166102.

[R2] H. Hu, X. Zhou, Y. Wang, et al. Efficient photocatalytic H_2 evolution over sulfoselenide $CuS_{0.5}Se_{0.5}$/g-C_3N_4 S-scheme heterojunction. Int. J. Hydrogen Energy, 2026, 214: 153834.

[R3] Y. Zheng, Q. Chen, J. Ouyang, et al. Manganese-Assisted Carbon Nitride/Carbon Nanoribbons Heterojunction for Efficient Photocatalytic H_2O_2 and H_2 Production. ChemSusChem, 2025, 18: e202500939.

[R4] P. Sarangi, K. Das, J. Sahu, et al. Structurally Modulated NiV-LDH with CdMoSe-Quantum Dots: Unlocking the Active Centers at S-Scheme Heterojunctions for Stimulating Photocatalytic H_2O_2 Production and H_2 Evolution. Inorg. Chem., 2025, 64(6): 2723-2736.

[R5] Y. Zhang, J. Su, Y. Wang, et al. Boosting Photocatalytic H_2 and H_2O_2 Evolution Enabled by Surface Non-Uniform Pyroelectric Field Derived Dielectrophoresis Effect. Adv. Energy Mater., 2025, 15: 2501097.

[R6] X. Zhou, S. Wu, L. Peng, et al. In-Situ Deposition of Red Phosphorus onto BN: A Metal-Free Heterojunction for Efficient Photocatalytic Pure Water Splitting to Produce H_2 and H_2O_2. ACS Sustainable Chem. Eng., 2025, 13: 21111-21121.

[R7] L. Biswal, D. P. Sahoo, U. A. Mohanty, et al. MXene Derived Ti_3C_2-TiO_2 Coupled NiCo LDH: A 2D/3D Interfacial Engineered S-Scheme Heterojunction for Enhanced Photocatalytic H_2O_2 and H_2 Production. Langmuir, 2025, 41: 23182-23197.

[R8] S. Dash, S. P. Tripathy, S. Subudhi, et al. A Visible Light-Responsive Mixed-Valence Bimetallic Eu-Zr MOF-Based Nanoarchitecture toward Efficacious H_2O_2 and H_2 Production. Ind. Eng. Chem. Res., 2025, 64: 5841-5853.

[R9] Q. Zhang, Y. Pang, S. Yuan, et al. Establishing dual hole transfer channels to achieve long-lived trapped holes for significantly enhancing the photocatalytic pure water splitting performance of $ZnIn_2S_4$. Mater. Today Chem., 2025, 50: 103217.

[R10] B. P. Mishra, S. Das, L. Biswal, et al. MXene Schottky Functionalized Z-scheme Ternary Heterostructure for Enhanced Photocatalytic H_2O_2 Production and H_2 Evolution. J. Phys. Chem. C, 2024, 128: 1921-1935.

[R11] J. Hu, J. Li, Z. Pu, et al. S-scheme NiO/C_3N_5 heterojunctions with enhanced interfacial electric field for boosting photothermal-assisted photocatalytic H_2 and H_2O_2 production. J Colloid Interf Sci, 2024, 665: 780-792.

[R12] H. Jiang, W. Ye, H. Zhen, et al. Novel 3D-on-2D g-C_3N_4/$AgIn_xS_y$ heterojunction photocatalyst for simultaneous and stoichiometric production of H_2 and H_2O_2 from water splitting under visible light. Chin. Chem. Lett., 2025, 36: 109984.

[R13] C. Li, X. Zhang, T. Song, et al. Interface-engineering derived WS_2/S-g-C_3N_4 nanosheet Z-scheme heterostructures towards enhanced photocatalytic redox and H_2O_2 generation. Environ. Chem. Eng., 2024, 12: 113396.

[R14] S. Baluchová, S. Zoltowska, P. Giusto, et al. Binaphthyl mediated low temperature synthesis of carbon nitride photocatalyst for photocatalytic hydrogen evolution. ChemSusChem, 2024, 17: e202400618.

[R15] Q. Ju, H. Huo, C. Huang, et al. Unlocking the photocatalytic overall water splitting ability of indium sulfide to produce H_2 and H_2O_2. Chem. Eng. Sci., 2024, 284: 119507.

[R16] S. Wu, S. Zhang, Q. Zhang, et al. Efficient Holes Abstraction by Precisely Decorating Ruthenium Single Atoms and RuO_x Clusters on $ZnIn_2S_4$ for Photocatalytic Pure Water Splitting. Small, 2024, 20: 2405153.

[R17] Q. Yang, R. Li, S. Wei, et al. Schottky functionalized Z-scheme heterojunction photocatalyst Ti_2C_3/g-C_3N_4/BiOCl: Efficient photocatalytic H_2O_2 production via two-channel pathway. Appl. Surf. Sci., 2022, 572: 151525.

[R18] B. P. Mishra, L. Acharya, K. Parida. Synergistic effect of exfoliation and substitutional doping in graphitic carbon nitride for photocatalytic H_2O_2 production and H_2 generation: a comparison and kinetic study. Catal. Sci. Technol., 2023, 13: 1448-1458.

[R19] K. Wang, J. Li, X. Liu, et al. Sacrificial-agent-free artificial photosynthesis of hydrogen peroxide over step-scheme WO_3/NiS hybrid nanofibers. App. Catal. B: Environ., 2024, 342: 123349.

[R20] Y. Xiang, Z. Xia, W. Hu, et al. Catechol-Formaldehyde Resin Coated CdS Core-Shell Composite as Robust Photocatalyst for Long-Term Sustainable Artificial Photosynthesis of H_2O_2. Chin. J. Chem. 2024, 42: 1975-1985.